On the effect of gas diffusion layers hydrophobicity on direct methanol fuel cell performance and degradation

F. Bresciani*, C. Rabissi, M. Zago, R. Marchesi, A. Casalegno

Politecnico di Milano, Department of Energy, Via Lambruschini 4, 20156 Milano, Italy

Received 25 July 2014
Received in revised form
2 September 2014
Accepted 23 September 2014
Available online 2 October 2014

1. Introduction

Direct methanol fuel cell (DMFC) is a promising technology for both remote stationary and portable applications mainly due to the use of a high energy-density liquid fuel [1–3]. Among the technical issues that still hinder the DMFC commercialization, mass transport phenomena management and a severe performance degradation are two of the mainly investigated [4–7]. DMFCs are fed with a liquid mixture composed by water and methanol; both of them flow through the membrane from the anode to the cathode. Water crossover through the membrane may cause problems such as cathode flooding and anodic water depletion. The former decreases oxygen diffusivity at cathode, determining a lower cell voltage, while the latter enhances methanol crossover through the membrane, implying fuel waste and performance loss. During the last years, both water and methanol crossovers in DMFCs have been extensively studied [5,9]. It has been found that the design of gas diffusion layer (GDL), usually coated with an additional micro porous layer (MPL), plays an important role in the management of mass transport phenomena. However, the investigation of DMFC mass transport phenomena evolution during lifetime and the effect of GDL configuration on DMFC degradation are only rarely presented [4].

DMFC degradation consists in two different components [6]: a temporary degradation, which can be recovered by means of apposite procedures, and a permanent one. Mass transport phenomena through a DMFC play a key role regarding various temporary degradation mechanisms already highlighted in the literature, such as both cathode electrode flooding and dehydration

* Corresponding author.
E-mail address: fausto.bresciani@polimi.it (F. Bresciani).

[10] or CO_2 gas-phase transport through the anode porous media [11] and along the anode flow field [12].

DMFC permanent degradation is attributed both to the electrodes and to the membrane; different degradation mechanisms have been highlighted, mainly from ex-situ investigations [6,7,13,14]. Electrochemical surface area (ECSA) loss can be due to phenomena such as platinum dissolution, ruthenium dissolution and crossover, carbon corrosion; besides, delamination and thinning of the membrane are sometimes highlighted as other interesting mechanisms. However, the influence of the mass transport phenomena evolution, caused by degradation phenomena, or variations, due to modifications in the MEA structure, on the DMFC permanent degradation mechanisms occurrence has not yet been investigated.

This work aims to investigate experimentally the effect of the GDL hydrophobic properties on DMFC performances and degradation, coupling mass transport and electrochemical measurements during two analogous degradation tests on similar MEA's provided by different GDL's. Moreover, a previously developed DMFC model [9,15] is used to support and integrate the interpretation of the experimental results.

2. Experimental methodology

2.1. Experimental setup and MEAs

The experimental setup for single DMFC characterization and degradation tests (both for overall and anode operation) is described in Ref. [4], where the set of equations governing mass transport and the recent improvements to the experimental setup are explained in details.

All the MEA's used for this work are manufactured by IRD Fuel Cell A/S. The reference MEA's (named "M–M") used for this work are commercial 25 cm^2: membrane is Nafion115, with catalyst loading of 1.8 mg cm^{-2} (PtRu) at the anode electrode and 1.2 mg cm^{-2} (Pt) at the cathode electrode. Both anode and cathode diffusion layer are Sigracet® SGL35DC (thickness 325 μm, 20% PTFE content, with MPL). The benchmark MEA's (named "G–M"), with the same active area, membrane and electrodes, presents differences from the reference one in the diffusion layers characteristics: anode GDL is Sigracet® SGL24BA (thickness 190 μm, 5% PTFE content, without micro-porous layer), while cathode diffusion layer is Sigracet SGL25B (thickness 235 μm, 5% PTFE content, with MPL).

During galvanic operation testing, unless differently indicated, anode and cathode are fed through a triple serpentine graphite flow field respectively with 1.0 M methanol solution with stoichiometry equal to 6 and air, saturated by water at ambient temperature, with stoichiometry equal to 3 both calculated at 0.25 A cm^{-2}. Instead, during anode operation tests, cathode is set as a dynamic hydrogen electrode, as explained in Ref. [11], feeding it with 3.5 Nml min^{-1} of dry hydrogen. Nominal current density is 0.25 A cm^{-2} and the fuel cell temperature is kept at 75 °C.

Data acquisition system continuously acquires at 0.5 Hz frequency. The voltage of the fuel cell is simultaneously measured by the electronic load and by a high precision acquisition board (NI 6210, estimated uncertainty: 1 mV) directly connected to the fuel cell, in order to have multiple readings. As a proxy for methanol crossover, CO_2 measurements are performed at the cathode exhaust with a Vaisala sensor GMP70 (uncertainty 50 + 2% ppm) in a vessel of 0.5 dm^3 volume provided with a liquid–gas gravity separator and a thermocouple (in order to evaluate the vessel saturation temperature). The obtained data are corrected by subtracting the measured ambient CO_2 concentration, thus the uncertainty of the final measurements is evaluated to be 70 + 2.8% ppm [22]. An heat exchanger to warm up the cathode exhaust to evaporate eventual liquid water and a thermo-hygrometer (Vaisala HMT333) for humidity (uncertainty 2%) and temperature (uncertainty 0.2 °C) measurements, located in a thermo-stated housing to avoid water condensation, permit to measure the water content in the cathode exhaust, as explained in Ref. [9]. The uncertainty associated to the measurement of water flow is evaluated equal to 7% in the whole investigated range [9].

2.2. Preliminary characterization

Prior to the degradation test characterization, a first sample of G–M MEA has been characterized, obtaining several polarization curves in various operating conditions; just few of them are reported in the followings for the sake of shortness. The same tests have been carried out on the M–M MEA acting as a reference, in order to highlight the effect of the modifications introduced in the GDL configuration. The preliminary characterization also allows ensuring the degradation tests results reliability, by means of a results repeatability evaluation.

The polarization curve acquisition is composed of 9 single measurement points, collected increasing current densities following one-way curves, as explained in Ref. [8]. Each polarization curve is performed with reactants at constant flow rates in order to ensure the steady state operation, in order to obtain high reliability of methanol crossover, water content in cathode outlet and EIS measurements.

Electrochemical impedance spectroscopies (EIS) are executed during the diagnostic polarization curves, at 0.1 and 0.25 A cm^{-2} steps, and periodically during the degradation tests, using a potentiostat/galvanostat (Autolab PGSTAT30) provided with a frequency response analysis module. The amplitude of the sinusoidal signal increases by increasing current density in order to provide a trade-off between the linear response in voltage and an adequate measurement quality [17,18]; thus, the imposed amplitude is adjusted so that the potential amplitude does not exceed 10 mV. The impedance is measured at frequencies included between 10 kHz and 50 mHz with a logarithmic distribution.

2.3. Degradation test

As explained in Refs. [19,20], a DMFC cannot work in continuous operation due to an excessive degradation rate and, for this reason, suitable operating strategies are adopted. In this work, the DMFC reference operating strategy consists in cycles of 20 min of effective operation, followed by 1 min of Refresh procedure. The Refresh is an IRD Fuel Cell confidential procedure similar to what reported in Ref. [18] to limit temporary degradation, consisting in an operation break during which a sequence of periods of OCV (about 0.8 V) and cathode air interruption (less than 0.3 V) are performed; as the operation restarts, a significant positive effect on performances is noticeable [19].

Besides, about every 100 h of this discontinuous degradation testing, a one-day interruption for diagnostic is performed. The diagnostic interruption is preceded and followed by a long break period (about 16 h) with the anode fed with a minimal fuel flow and the cathode closed; this procedure allows a complete removal of temporary degradation effects.

During the diagnostic operation interruptions, the DMFC degradation is evaluated performing polarization curves, EIS and, finally, cathode Cyclic Voltammetry (CV) to estimate the catalyst active area of the electrode. During CV measurement, dry hydrogen (3.5 Nml min^{-1}) and fully humidified nitrogen (0.6 Nl min^{-1} saturated at 80 °C) are fed to the anode and cathode compartments respectively and the cell is kept at 75 °C. The anode is taken as reference and counter electrode, while the cathode is taken as the

working one; its potential is continuously scanned back and forth between 0.05 V and 0.6 V with a scan rate of 25 mV s^{-1}. The cathode ECSA is then estimated considering the positive current density peak related to the hydrogen desorption [20]; this estimation is done assuming that the cathode catalyst is covered by a monolayer of hydrogen with a charge density of 210 μC cm^{-2}.

The overall permanent degradation is evaluated from the polarization curves as the voltage decay at reference current (i.e. 0.25 A cm^{-2}), from the beginning to the end of the test, divided by the test duration.

3. Preliminary characterization

To highlight the influence of the modified GDL configuration on performance, as described in paragraph 2.1 the benchmark MEA's (G–M) have been provided with key differences in the GDL hydrophobicity: in comparison with the reference configuration, the PTFE content in both the GDLs has been sensibly reduced (from 20% to 5%) and the anode MPL has been removed. These modifications are intended to determine a higher water crossover through the membrane and increase the onset of cathode flooding probability.

Fig. 1 reports both the galvanic and anode polarization curves in the same reference conditions for the two investigated MEA's. The anode polarizations reveal that the MPL removal does not seem to affect the anode overpotential: the two MEA's show similarities in anode performance due to the same electrode configuration. A GDL without MPL has a higher diffusivity and a lower permeation threshold in comparison to a GDL coated with MPL [21]; this results in an increase of water and methanol concentration at the anode electrode, that could determine an anode overpotential improvement only in case of mass transport limited regime. Thus, the reported anode polarizations seem to be mainly kinetically-dominated on the whole current density range, while the effect of the mass transport limitations losses appears to be less important. This is clearly related with the high anode stoichiometry suggested by the manufacturer: indeed, the lowest stoichiometry, obtained at the highest current density, is still high, equal to 3.75.

However, despite the unchanged anode performance between the two MEA's, the polarization curves in reference conditions, reported in Fig. 1, show that the M–M MEA has better overall performances than the G–M MEA on the total range of current densities. Particularly, an important drop of the G–M MEA performance is clear for current densities higher than 0.25 A cm^{-2}: the lack of the anode MPL could probably determine both an increase in methanol crossover and an easier cathode flooding, also promoted by the low cathode stoichiometry value, 3 at 0.25 A cm^{-2}, suggested by the manufacturer. Indeed, these polarization curves seem to show for the G–M MEA severe mass transport limitations at the cathode, as evident from the change in the curve slope at high current densities, when both water drag through the membrane and water production at the cathode are strongly enhanced.

Fig. 2 reports methanol crossover and water content measurements at the cathode outlet, acquired during the galvanic polarization curves of Fig. 1. As follows, the modifications introduced in the GDLs configuration between M–M and G–M MEA's seem to determine significant modifications in the DMFC mass balances.

Particularly, from the methanol crossover curves it is observable that:

- at low current densities, in the G–M MEA a slight increase in methanol concentration at the anode electrode is probably present, which results in an increase in methanol crossover through the membrane. This is related to a decrease in the anode GDL mass transport resistance, due to the reduction in GDL's hydrophobicity and to the absence of anode MPL;
- moving towards high current densities, the crossover rate difference between the two MEAs further decreases; this is coherent with a progressive decrease of methanol concentration in the anode electrode, due to the increasing of its consumption rate, i.e. the current density, at constant reactants flows. Therefore methanol crossover increase seems not to justify the magnitude of performance drop evident in the galvanic polarization curves of Fig. 1;

For what concerns the water flux measured in the DMFC cathode exhaust:

- at low current densities, the G–M MEA shows a higher water content in cathode outlet than the M–M one; since until 0.25 A cm^{-2} the cathode water flux of G–M MEA remains approximately constant, it is governed by diffusion mechanisms [21]. The lower water flux of the M–M MEA is related to a greater water transport resistance from anode to cathode, due to the presence of the anode MPL and to a higher GDL's hydrophobicity;

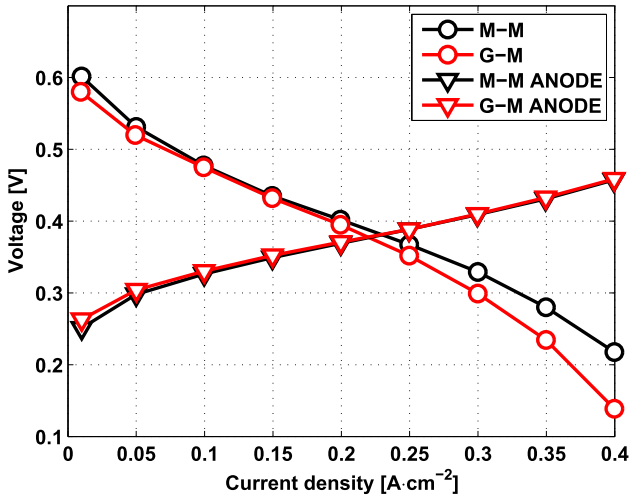

Fig. 1. Anode and overall polarization curves comparison between M–M and G–M MEAs in reference condition.

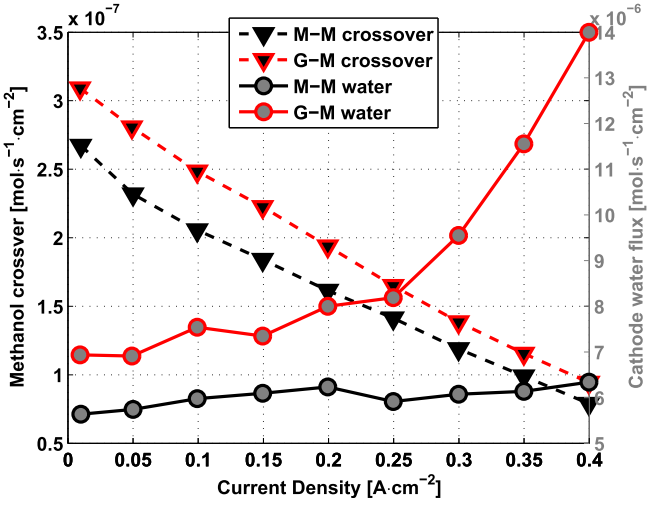

Fig. 2. Methanol crossover and cathode water flux comparison between M–M and G–M MEAs during polarization curves in reference condition.

- increasing the current density over 0.25 A cm^{-2}, the G–M MEA shows a sudden and strong change in the water transport regime, while the M–M MEA does not reveal significant variations. These results are very similar to those reported in Ref. [15]. Since the maximum diffusive water transport through a GDL is governed by the saturation concentration, this strong increase in water flux cannot be attributed to diffusion mechanism. The breakthrough is most probably due to liquid water permeation through the G–M cathode GDL [21], which is related to an increase of liquid water content and flow in cathode electrode. Such flooding effect, hindering oxygen transport towards the active sites, is the major cause of the mentioned performance reduction at high current. On the contrary it is not present in the M–M MEA: the water content in the cathode electrode is not enough to breakthrough the cathode GDL, because of both higher cathode GDL hydrophobicity and lower anode electrode water concentration, caused by MPL absence.

The comparison between the EIS performed during the galvanic polarization curves of Fig. 1 at 0.1 and 0.25 A cm^{-2}, reported in Fig. 3, further confirms the proposed interpretation:

- at low current density, the impedance spectra shape for both MEA's is rather similar at low frequencies, where an inductive loop attributable to anode [16] is clear. This behavior is similar for the two MEA's, confirming that the G–M and M–M anodes do not show significant differences, coherently with the anode polarizations of Fig. 1. Instead, strong differences are evident in the medium frequencies region, associated to the phenomena occurring at cathode side. The reference MEA presents two easily identifiable circles, while the G–M MEA spectrum is altered by oxygen transport limitation caused by both higher water content in the cathode electrode and hindered methanol crossover, Fig. 2;
- at high current density, 0.25 A cm^{-2}, where the change in water transport regime occurs, Fig. 2, the differences between the two MEAs spectra in the mid-frequencies range are even more pronounced. Moving towards the low frequencies zone, very strong disturbances related to mass transport limitations are observable in the G–M MEA spectrum, while they are less evident in the M–M one. Therefore EIS confirms that the cathode electrode effectively operates in flooding conditions: a hindered oxygen transport toward the active sites is evident [22], determining the strong performance loss of the G–M MEA observed in Fig. 1.

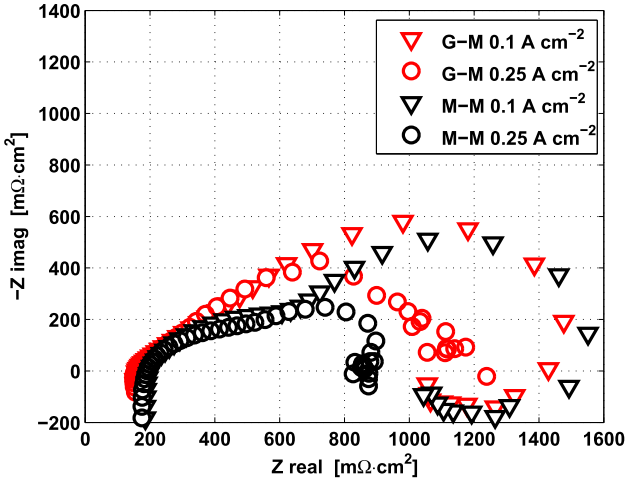

Fig. 3. EIS comparison between M–M and G–M MEAs during polarization curves in reference condition.

Hence, the comparison between the preliminary characterizations of the two MEA's clearly shows that the GDL configuration adopted for the G–M MEA promotes the flooding of the cathode electrode, resulting in cathode performance losses and increase in the cathode water flux. EIS analyses further confirm this interpretation because cathode flooding appears as a severe mass transport limitation, in the medium frequencies characteristic of cathode phenomena.

3.1. Model validation

In this paragraph an already developed 1D + 1D DMFC model [9,15] has been used to analyze the previously described experimental results. Particularly, flooding effects are modeled considering two contributions [9]:

- Superficial pores obstruction due to water condensation on GDL interface facing to the channel. This effect is considered as a reduction of GDL effective diffusivity $D_{eff,GDL}$ proportional to liquid water concentration:

$$D_{GDL} = D_{eff,GDL} - C_1 \cdot \left(\overline{C}_{H_2O} - C^{sat}_{H_2O}\right)^{0.58} \quad (1)$$

where $\overline{C}_{H_2O}$ is the time-averaged total water concentration in the cathode channel, $C^{sat}_{H_2O}$ is the saturation value, D_{GDL} is GDL diffusivity and C_1 is derived from model validation.

- Bulk pores obstruction caused by the establishment of liquid pathways through the GDL. This implies a reduction of $D_{eff,GDL}$ proportional to liquid water permeation through cathode GDL, $N_{GDL,perm}$:

$$D_{GDL} = D_{eff,GDL} - C_2 \cdot \left(N_{GDL,perm}\right)^{C_3} \quad (2)$$

where C_2 and C_3 are obtained by model validation.

Moreover, the model is validated at the same time with respect to different typologies of measure: anode polarization, polarization, methanol crossover and water content measured at cathode outlet. In this way all the main physical phenomena are described with a reduced uncertainty: a similar approach has been already presented in Ref. [15]. For the sake of shortness in this work only the comparison between measured and simulated performance with and without flooding effects are reported (Fig. 4).

Considering the M–M MEA the models with and without flooding effects are effectively superimposed, indicating that flooding does not occur. Instead, in G–M MEA, where flooding is expected as previously discussed, a relevant difference is evident at high current densities omitting flooding effects. Model simulations emphasize that flooding onset occurs at nearly 0.25 A cm^{-2}, coherently with the experimental measures of water transport, where a sharp increase in water flux at cathode outlet is observable just around 0.25 A cm^{-2}, Fig. 2.

The presented modeling analysis further confirms that, in the investigated operating conditions, the performance of G–M MEA is hindered by cathode flooding.

4. DMFC degradation test

Fig. 5 reports the voltage decay comparison between the M–M and the G–M MEA's during 420 h of degradation test based on refresh cycles; each operation interruption, noticeable approximately every 100 h, corresponds to a break for diagnostics, preceded and followed by the temporary degradation removal procedure already explained in paragraph 2.3.

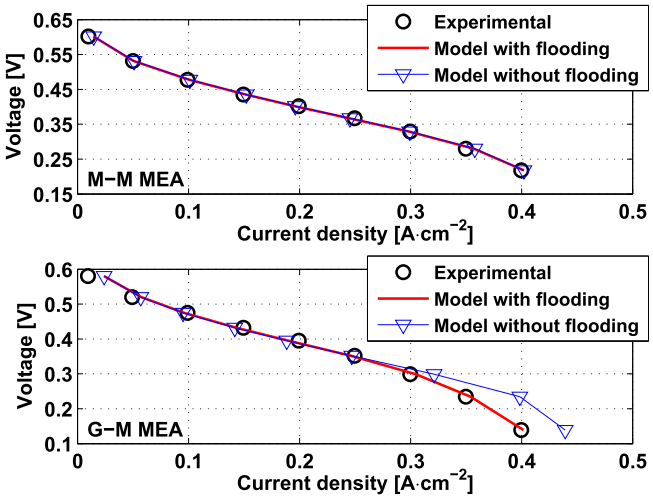

Fig. 4. Comparison of simulated performance of M–M and G–M MEAs with and without flooding effects.

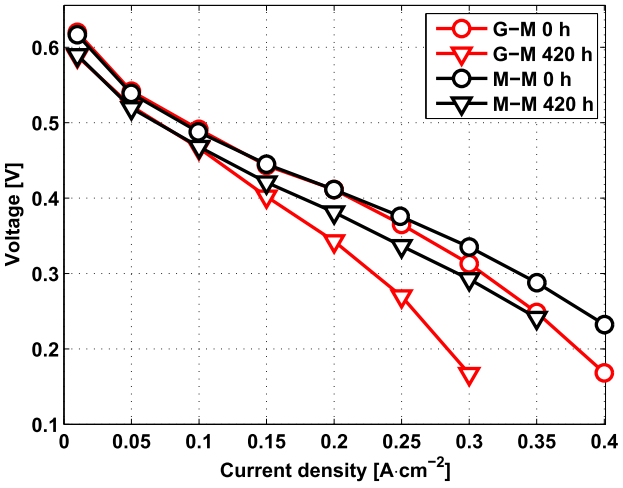

Fig. 6. Polarization curves comparison between M–M and G–M MEAs at the beginning and at the end of the galvanic discontinuous degradation tests.

The shape of the voltage decay for the M–M MEA appears more regular and each interruption for diagnostic determines a strong performance recovery, while the G–M MEA shows a more unstable voltage decay curve. Besides, after each operation region, the diagnostic break determines a less continuous recovery in comparison with its effect on the M–M MEA performance. Particularly, the first 100 h operation period corresponds to a very strong degradation for G–M MEA, at the end of which, in addition, the performance does not show any significant recovery with the diagnostic interruption; this behavior continues until 150 h of test and then it shows stabilization. Hence, an important event, determining a permanent performance loss, has probably occurred during the first 100–150 h of operation of the G–M MEA.

The polarization curves, performed during the interruption for diagnostic at the beginning and at the end of the two degradation tests, are reported in Fig. 6. At the beginning of the test, at high current densities, the M–M MEA shows higher performance than the G–M MEA, as already discussed. The polarization curves performed at the end of the test, further confirm the stronger permanent degradation that the 420 h test determines onto the G–M MEA performance, 227 μV h^{-1}, than onto the M–M one, 94 μV h^{-1}, as just seen in Fig. 5.

An interesting insight is obtainable from Fig. 7, which reports the EIS acquired in reference conditions, 0.25 A cm^{-2}, during the polarization curves reported in Fig. 6. As already presented in the preliminary characterization, the G–M MEA spectra present a less distinguishable electrode semicircles respect to the M–M MEA spectra, which is due to the mass transport limitations at the cathode, already attributed to flooding. Both the MEA's, moving towards the end of the test, show a worsening in mass transport limitations determining an increase in the total resistance. This, for the M–M MEA, results in slight disturbances at low frequencies; differently, the total resistance of G–M MEA presents a very strong increase, which is most probably caused by a strong enhancement of mass transport limitations at the cathode.

During each diagnostic interruption, cyclic voltammetry analyses are performed: the plot of the CV's related to the beginning and to the end of the degradation test for both the MEA's are reported in Fig. 8, together with the detail of the sensibly decreasing hydrogen desorption peaks. From these analyses, it is possible

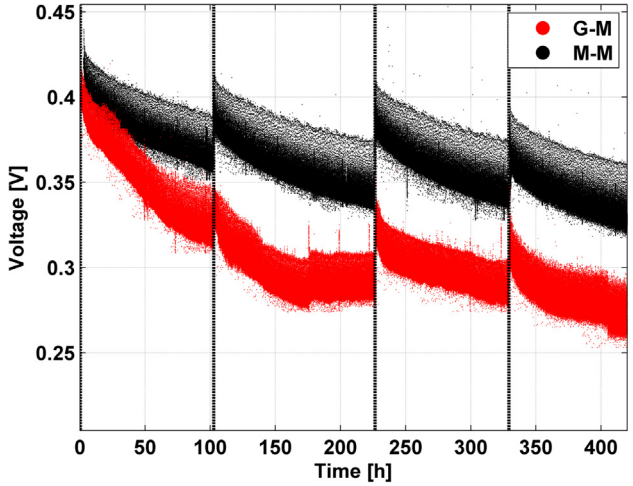

Fig. 5. Voltage decay comparison between M–M and G–M MEAs during galvanic discontinuous degradation tests.

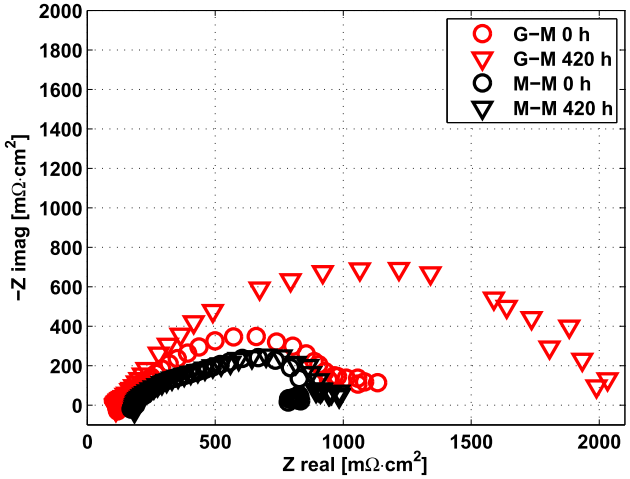

Fig. 7. Comparison between the M–M and G–M MEAs EIS during polarization curves at beginning and end of the galvanic discontinuous degradation tests.

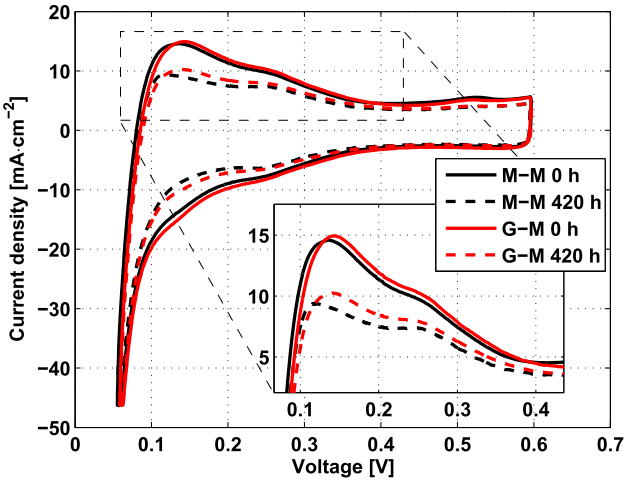

Fig. 8. CV plots performed during the first and the last diagnostic break, for M–M and G–M MEAs, with detail of the H2 desorption peaks.

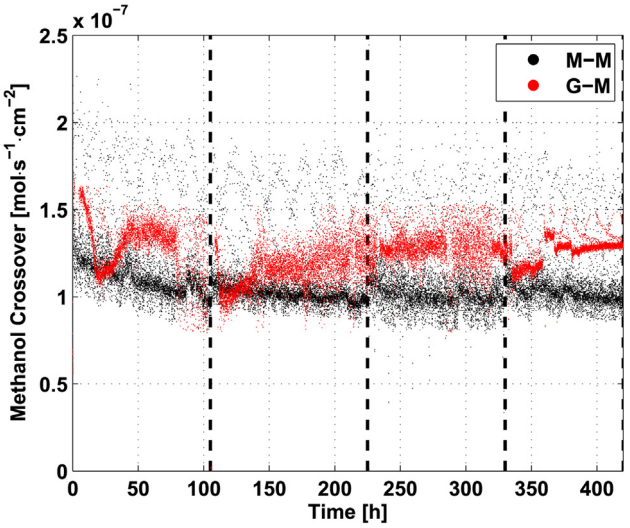

Fig. 10. Methanol crossover trend comparison between M–M and G–M MEAs during galvanic discontinuous degradation tests.

estimate the Electro-Chemical Surface Area (ECSA) progress during the degradation test shown in Fig. 5.

The comparison between the M–M and G–M MEA's cathode electrochemical active surface trend during the degradation test is reported in Fig. 9. It is well known that the cathode ECSA loss, related to the typical electrode degradation mechanisms, is one of the main causes for DMFC degradation. The degradation test determines, for both the MEA's, a comparable ECSA loss of about 30% from the initial values, and its decay does not highlight significant differences; this means that the dissimilarities in the mass balances between the two MEA's seems to not influence the cathode ECSA loss mechanisms. For this reason, it is possible to exclude that the variation in the G–M MEA spectra, Fig. 7, was directly related to a permanent ECSA loss.

To deepen the mass transport related phenomena evolution, Figs. 10 and 11 report respectively the methanol crossover and cathode water flux evolution in time for the M–M and G–M MEA's during the degradation test.

Methanol crossover for the M–M MEA, Fig. 10, presents a regular behavior in time: it slightly decreases during each part of the test, while each operation interruption for diagnostics partially recovers its value, coherently with [8]. Instead, the crossover measured for the G–M MEA reveals a very unstable behavior with a slightly higher average value than the reference one, coherently with Fig. 2; this seems to imply a strongly unsteady operation of the G–M MEA cathode, but this difference appears so small not to justify the strong performance loss during the initial part of the test.

More interesting, as expectable, is the behavior of the cathode water flux acquired during the degradation test, reported in Fig. 11. Indeed, during the first 150 h of operation, a strong and progressive increase of water content in the cathode exhaust is noticeable for the G–M MEA, while the water content in M–M MEA cathode outlet remains about constant during the entire degradation test. This rising is simultaneous with the performance loss seen in Fig. 5 and it is most likely due to the progressive breakthrough of the cathode GDL and the consequent electrode flooding. Such event interestingly occurs during the very first period of operation, the water content measured value tends then to stabilize around an average value three times higher than the M–M one. The evolution

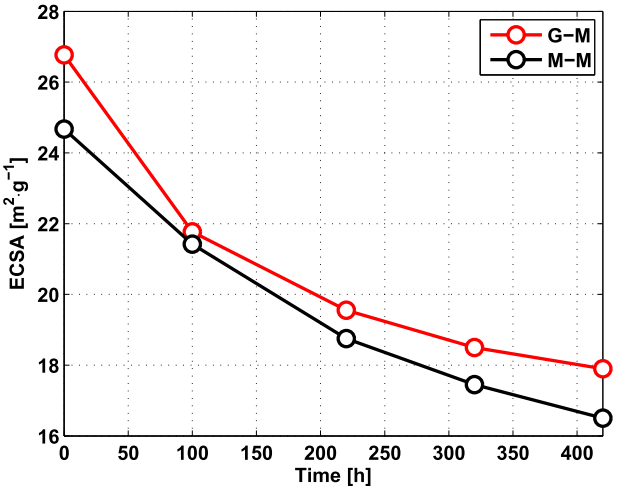

Fig. 9. Comparison between the M–M and G–M MEAs ECSA measured during the galvanic discontinuous degradation tests.

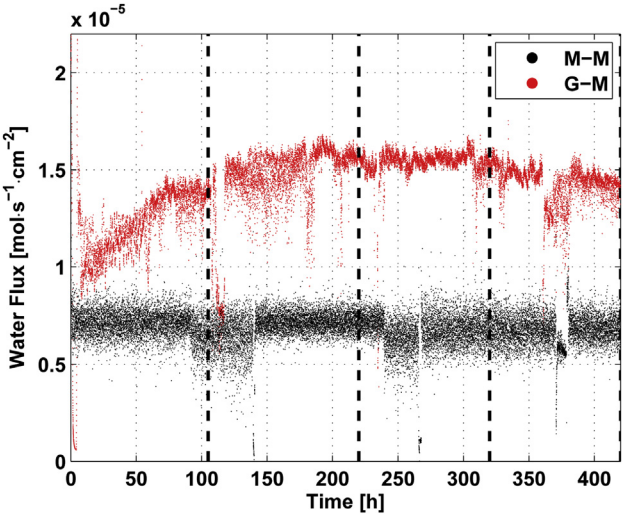

Fig. 11. Cathode water flux trend comparison between M–M and G–M MEAs during galvanic discontinuous degradation tests.

of the water content in the cathode outlet could be due to a modification of the GDL's transport properties in the G–M MEA, while the GDLs' of the M–M MEA seems not to be significantly influenced by the degradation test.

Methanol and water transport is characterized also during the polarization curves; in The cathode water flux acquisitions during the first, second and last polarization curves are reported in Fig. 12. The interesting trend permit to confirm that, while for the reference M–M MEA the water balance maintains approximately constant on the whole current density range and during the entire degradation test, for the G–M MEA the most important phenomena occur during the very first operation period. Indeed, after the first 100 h of operation, the cathode water flux shows a strong modification: at 0.25 A cm^{-2}, the water expelled in the cathode exhaust is increased by 50%. The change in the cathode GDL properties during the degradation test determines an increase of overall diffusion coefficient and the onset of liquid permeation at lower current density.

Hence, a considerable modification of mass transport phenomena in the G–M MEA occurs during the test, but it does not affect significantly the degradation mechanisms, as confirmed by the similar cathode ECSA loss in the two MEA's.

Particularly, it is possible to propose the following interpretation, regarding the effect of the cathode mass transport limitations, due to flooding, on the permanent degradation:

- considering the same current density, a significant decrease in cathode ECSA implies an increase of oxygen flux, specific to active area, towards the active sites. The higher the oxygen flux, the lower the local oxygen concentration on the active surface, resulting in a cathode overpotential increase;
- the flooding of the cathode electrode results in a decrease of the effective oxygen diffusivity, as in Ref. [9]; at constant current density and, thus, constant oxygen flux in the electrode, such diffusivity reduction implies a decrease of local reactant concentration on the active area and an increase of cathode overpotential;
- in the G–M MEA the effect of ECSA loss is strongly worsened by the increase of cathode flooding: the coupled phenomena determine severe mass transport limitation and a higher degradation rate compared to the M–M MEA. Indeed, the oxygen concentration on the active surface is reduced by both phenomena, implying a combined effect on the cathode overpotential.

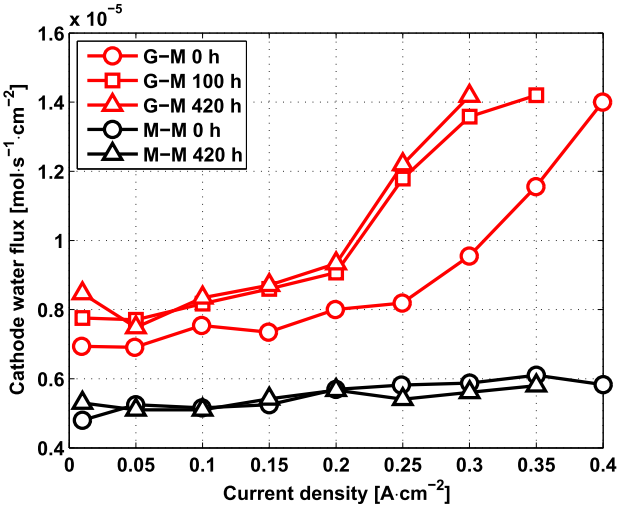

Fig. 12. Evolution of water content at cathode outlet in M–M and G–M MEAs during polarization curves at BoT and EoT.

Coherently with this interpretation, the mass transport limitations effects during the M–M MEA degradation test are less pronounced.

5. Preliminary modeling interpretation

The validated model is finally used as a diagnostic tool to analyze the proposed origins of the different degradation rates of M–M and G–M MEA's.

To achieve this, the same decrease of cathode ECSA is introduced in both G–M and M–M MEA models as a reduction of cathode exchange current density [23]:

$$i_c^* = i_{c,0}^* \cdot \left(\frac{\mathrm{ECSA}_t}{\mathrm{ECSA}_0}\right) \tag{3}$$

where $i_{c,0}^*$ is the exchange current density at the BoL (Begin of Life) and $\mathrm{ECSA}_t/\mathrm{ECSA}_0$ is the ratio between the catalyst active area at the considered time and the one at the BoL.

Moreover, the ECSA reduction could strengthen flooding, because the water production is concentrated on a lower active surface, increasing the water concentration in the pores close to the active sites. Therefore the previously developed correlation, including the effect of liquid permeation through cathode GDL, has been properly modified considering ECSA reduction:

$$D_{\mathrm{GDL}} = D_{\mathrm{eff,GDL}} - C_2 \cdot \left(\frac{\mathrm{ECSA}_0}{\mathrm{ECSA}_t}\right)^{\beta} \cdot \left(N_{\mathrm{GDL,perm}}\right)^{C_3} \tag{4}$$

where C_2, C_3 and β are fitting parameters. The proposed correlations (Eqs. (3) and (4)) do not pretend to provide a detailed and exhaustive description of such complex phenomenon, but a tool to increase its understanding and set the basis for further studies.

Fig. 13 reports the simulated performance with and without the effect of cathode ECSA reduction on flooding. Considering MEA M–M, the model without the effect of ECSA reduction on flooding results in a downward translation of the whole polarization curve:

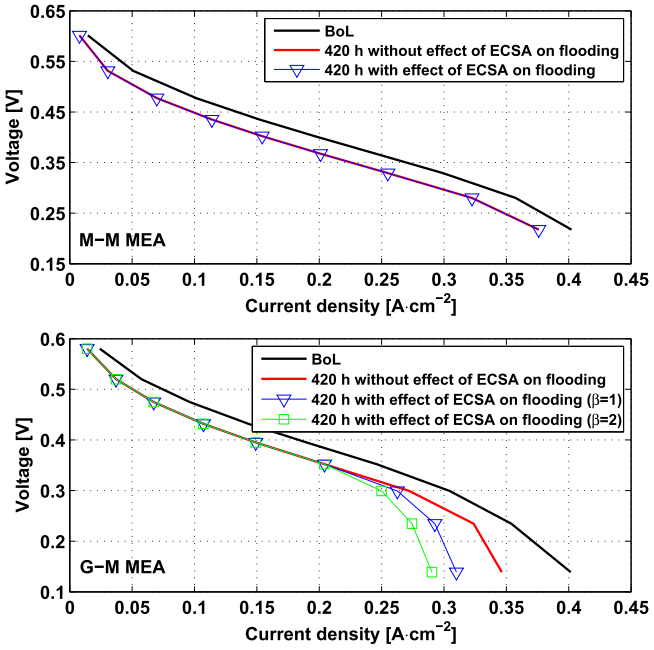

Fig. 13. Simulated performance of M–M and G–M MEAs with and without the effect of cathode ECSA reduction on flooding.

this is caused by the decrease of the exchange current density. Instead the model with the effect of ECSA reduction on flooding is superimposed to the previous one: this confirms that in M–M MEA no liquid permeation through cathode GDL occurs.

Considering G–M MEA, the model without the effect of ECSA reduction on flooding presents a voltage loss similar to M–M MEA, a part form the sharp decrease of performance around 0.32 A cm^{-2}. This behavior is caused by the increased water flux at cathode outlet (i.e. flooding magnitude) after 420 h of operation, as already highlighted in Fig. 12. Anyway such model is not able to reproduce the significant performance reduction observed in the experimental data, Fig. 6. The simulated performance with the effect of ECSA reduction on flooding, assuming a β value included between 1 and 2, presents a considerable voltage decrease with the increasing current: this result qualitatively reproduces the experimental observations of Fig. 6. These results suggest that ECSA loss could effectively increase electrode flooding locally close to the active sites.

6. Conclusions

This work presents an experimental and modeling analysis of the effect of the GDL's hydrophobicity on DMFC performances, mass transport phenomena and degradation; the analysis has been carried out through the comparison of two similar MEA's, if excluded for the GDL configuration. Particularly the G–M MEA presents a lower GDL's PTFE content and an anode GDL without MPL, while the M–M MEA presents an anode GDL with MPL and higher hydrophobic properties; the experimental and modeling investigations permit to draw the following conclusions:

- the G–M MEA presents a higher degradation rate and a less stable operation than the M–M MEA; both these aspects seem to be related to a difficult management of mass transport phenomena. Particularly, a strong initial degradation is observable for the G–M MEA and it is related to a strong increase in cathode water flux;
- the ECSA loss of both the MEA's is comparable, but the permanent degradation rates are significantly different; this is probably due to the coupling effect of ECSA loss with significant cathode mass transport limitations due to electrode flooding;
- a higher GDL's hydrophobicity and the anode MPL presence determine a strong improvement in the DMFC performances, which is mainly due to a more appropriate cathode operation. A lower methanol crossover and, especially, a lower cathode water flux can explain such enhancement. In fact the cathode of the G–M MEA operates in flooding conditions;
- a preliminary MEA's characterization, coupling performance and mass transport measurements, turns out to be fundamental to correctly analyze the degradation tests performed on both MEA's;
- MEA model predictions, able to reproduce qualitatively the experimental data, confirm that, when the cathode is flooded, a certain decrease of ECSA determines a more relevant voltage loss. suggesting that ECSA loss could increase electrode flooding locally close to the active sites.

Acknowledgments

This work has been performed in the frame of the FCH-JU FP7 project Premium Act (EC Grant Agreement 256776). The authors would like to thank Matteo Sanarico for the helpful support in the experimental measurements.

References

[1] S.K. Kamarudin, F. Achmad, W.R.W. Daud, Int. J. Hydrogen Energy 34 (2009) 6902–6916.
[2] P. Agnolucci, Int. J. Hydrogen Energy 32 (2007) 4319–4328.
[3] X. Li, A. Faghri, J. Power Sources 226 (2013) 223–240.
[4] A. Casalegno, C. Santoro, F. Rinaldi, R. Marchesi, J. Power Sources 196 (2011) 2669–2675.
[5] Y. Tian, G. Sun, Q. Mao, S. Wang, H. Liu, Q. Xin, J. Power Sources 185 (2008) 1015–1021.
[6] H. Cha, C. Chen, J. Shiu, J. Power Sources 192 (2009) 451–456.
[7] L.S. Sarma, C. Chen, G. Wang, K. Hsueh, C. Huang, H. Sheu, D. Liu, J. Lee, B. Hwang, J. Power Sources 167 (2007) 358–365.
[8] A. Casalegno, F. Bresciani, M. Zago, R. Marchesi, J. Power Sources 249 (2014) 103–109.
[9] M. Zago, A. Casalegno, C. Santoro, R. Marchesi, J. Power Sources 217 (2012) 381–391.
[10] J. Park, M.A. Scibioh, S. Kim, H. Kim, I. Oh, T.G. Lee, H.Y. Ha, Int. J. Hydrogen Energy 34 (2009) 2043–2051.
[11] F. Bresciani, A. Casalegno, M. Zago, R. Marchesi, Fuel Cells 14 (2014) 386–394.
[12] H. Yang, T. Zhao, Q. Ye, J. Power Sources 139 (2005) 79–90.
[13] P. Liu, G. Yin, K. Cai, Electrochim. Acta 54 (2009) 6178–6183.
[14] W. Chen, G. Sun, J. Guo, X. Zhao, S. Yan, J. Tian, S. Tang, Z. Zhou, Q. Xin, Electrochim. Acta 51 (2006) 2391–2399.
[15] M. Zago, A. Casalegno, F. Bresciani, R. Marchesi, Int. J. Hydrogen Energy (2014), http://dx.doi.org/10.1016/j.ijhydene.2014.03.147.
[16] S.K. Roy, M.E. Orazem, B. Tribollet, J. Electrochem. Soc. 154 (2007) B1378–B1388.
[17] E. Barsoukov, J.R. Macdonald, Impedance Spectroscopy. Theory, Experiment, and Applications, second ed., Wiley and Sons, 2005.
[18] S.J. Bae, S. Kim, J.I. Park, J. Lee, H. Cho, J. Park, Int. J. Hydrogen Energy 35 (2010) 9166–9176.
[19] F. Bresciani, A. Casalegno, J.L. Bonde, M. Odgaard, R. Marchesi, Int. J. Energy Res. 38 (2014) 117–124.
[20] H. Wang, X.Z. Yuan, H. Li, PEM Fuel Cell Diagnostic Tools, CRC press, 2012.
[21] F. Bresciani, A. Casalegno, G. Varisco, R. Marchesi, Int. J. Energy Res. 38 (2014) 602–613.
[22] A. Casalegno, F. Bresciani, G. Groppi, R. Marchesi, J. Power Sources 196 (2011) 10632–10639.
[23] S. Jomori, N. Nonoyama, T. Yoshida, J. Power Sources 215 (2012) 18–27.